J. Plasma Physics (2005), *vol.* 71, *part* 5, *pp.* 589–609. © 2005 Cambridge University Press
doi:10.1017/S0022377804003332 Printed in the United Kingdom

Simulation study of the effect of recombination processes in an expanding plasma

TUDOR NEDELEA, BORIS BRIEHL
and HERBERT M. URBASSEK

Fachbereich Physik, Universität Kaiserslautern, Erwin-Schrödinger-Straße,
D-67663 Kaiserslautern, Germany
(urbassek@rhrk.uni-kl.de)

(Received 8 December 2003, revised 26 July 2004 and accepted 30 July 2004)

Abstract. Using particle-in-cell computer simulation, the processes occurring in a plasma formed by isothermal evaporation of ions and electrons off a planar wall are studied. A simple model to implement three-body recombination is introduced into this scheme; it fulfills momentum and energy conservation and obeys the well-known dependences of the recombination rate on density and temperature. Ion acceleration processes are investigated, during both the particle emission phase and afterwards, during expansion into vacuum. Recombination strongly enhances ion acceleration, since due to the recombination-heated electron subsystem the expansion-front space-charge field is increased. Spatial segregation of the neutral gas cloud and the plasma cloud is demonstrated.

1. Introduction

After short-pulse laser irradiation of a target surface, a plasma cloud is formed in front of the surface, which consequently expands away from the surface [1–3]. The plasma-kinetic processes occurring during expansion are quite complex [4–12]. While the bulk of the cloud swiftly becomes quasi-neutral, a space-charge field develops at the expansion front; as a consequence, the ions in the cloud are accelerated at the cost of cooling the thermal energy of the electrons. Collision processes in the plasma may modify this simple picture. While most elastic, and also inelastic, collisions may be appropriately understood as a *friction* force in a hydrodynamic modelling [9], the occurrence of *recombination* processes may lead to qualitatively novel features [10, 13, 14]. In addition to a change in the charge-state distribution of the plasma, three-body recombination changes the number of particles in the plasma and hence invariably increases the energy per particle. The latter effect is enhanced by the release of recombination energy that locally heats the plasma.

Measurements on laser-induced plasma expansion usually detect the particle characteristics at the end of the expansion process, far away from the target. Here is where the charge-state distribution, the angular distribution, and the (charge-state resolved) energy distribution of the ions could be measured [2, 3, 15].

https://doi.org/10.1017/S0022377804003332 Published online by Cambridge University Press

An interesting result of such experiments is the observation of a strong positive correlation of the mean ion energy with the ion charge state [1–3, 15]. This experimental result gives evidence of a *segregation* of the plasma cloud into its various charge-state components. It has been argued that such a segregation may result from the self-consistent electrostatic fields accelerating the ions in the plasma [16, 17]. However, another approach relates the segregation to the recombination processes occurring in the plasma [10, 18]. Since the recombination rate depends nonlinearly on the electron density, and even more strongly on the electron temperature, recombination is strongest close to the emitting surface and in the center of the cloud, and vanishes towards the expansion front. Thus, the surviving highly-charged ions will be situated at the front, where the space-charge field and the consequent acceleration are strongest. Recombined ions will be found closer to the backside and the center of the cloud, with consequently weaker acceleration fields. As a result, the developing spatial segregation is accompanied by a different acceleration of the various ion species, which may explain the experimentally observed correlation mentioned above.

Understanding the temporal evolution of the charge-state distribution in the expanding cloud and the accompanying acceleration processes is of interest for many applications of laser-induced plasmas. As a prominent example, we mention pulsed-laser deposition, where the ablated particles are deposited on a substrate to grow a thin film [15]. Here an understanding of the energy distribution of the depositing ions is of prime interest for the thin-film structure, since the ion energy determines the incorporation probability, defect generation, etc., in the growing film.

In the present paper we perform a model simulation to understand the influence of recombination processes on the expansion characteristics of a plasma. While in the literature hydrodynamic simulations are usually employed to study the expansion of laser-induced plasmas, here we wish to explore the possibilities that a kinetic simulation scheme – the particle-in-cell (PIC) code [19] – offers. It is a self-consistent kinetic scheme that allows one to simulate the ion and electron distribution functions in the case of strong deviations from local thermodynamic equilibrium; this will be important, for example, in the plasma expansion front. The code allows most interaction and collision processes occurring in the plasma to be included; in the present paper, however, we shall restrict the simulation to the following assumptions.

(1) Dictated by computer time considerations, we only follow the expansion for a short time after the end of the laser pulse. During this time, however, the vast majority of recombination events will have occurred.

(2) A one-dimensional geometry will be adopted, i.e. the expansion will occur only perpendicular to the target surface. This is justified for the short times considered. For the same reason, the ion flow is also set equal to the electric flow, i.e. the net electrical current vanishes.

(3) The initial distributions of electrons and ions are strongly simplified. Electrons and ions are assumed to be emitted from the surface with a (half-)Maxwellian distribution and identical temperatures. Furthermore a fully ionized plasma, containing no neutrals, is assumed to be emitted. While these assumptions will not be fulfilled in a realistic plasma, they provide a simple scenario for the simulation model.

https://doi.org/10.1017/S0022377804003332 Published online by Cambridge University Press

(4) Electron–electron, electron–ion and ion–ion collisions are included in the PIC-scheme insofar as they are modelled by the self-consistent electrical field generated by the charged particles. In addition, we only include three-body recombination. Other collisions occurring in a real plasma are neglected in order to focus exclusively on the effect of recombination processes. We mention that the effect of ion–neutral and electron–neutral collisions will be friction-like, and will tend to adapt the velocities of the respective particle species. The effect of the electron impact ionization collisions of neutrals has been neglected. While ionization will counteract the effect of recombination, we have summarized its influence already in our strongly idealized initial condition, where we start with a fully ionized plasma.

(5) Angular scattering effects in charged-particle collisions are not included in the PIC code. Note that a one-dimensional PIC code, such as that used in the present work, deals with charge sheets, and not charge points. Furthermore, due to the introduction of a spatial cell structure, all collision effects within a cell are lost. We note that the addition of Coulomb collisions to PIC codes is possible, albeit at considerable computational cost [20]. The inclusion of the details of the Coulomb collision processes will change the thermalization behavior of electrons and ions, but not the space and time dependence of the electrostatic fields which lead to the ion acceleration and charge-state segregation processes studied in the present work.

To summarize, while each of the above model assumptions can be relaxed, we prefer to work in this idealized scenario in order to clearly demonstrate the effects of recombinations on an expanding plasma flow. This procedure will allow us to study the plasma expansion in scaled variables, cf. Sec. 3.3. An example of plasma parameters where our model applies is given by picosecond laser ablation of a metal target.

We note that in previous plasma modelling and simulation approaches that include recombination processes, as a rule only a rate-equation approach is used. Different levels of sophistication have been reached ranging from a homogeneous plasma [18, 21] to spatial one-dimensional time-dependent approaches [10], to the coupling of rate equations for the ionic component with a Fokker–Planck kinetic description of the electronic component [22]. A fully kinetic treatment of the electron and ion component, such as is attempted here, only rarely appears to have been performed [23, 24].

Section 2 summarizes the model studied and the simulation procedure. Three-body recombination is introduced into this scheme in a simple way, which however preserves the equilibrium rates, momentum conservation, and – apart from the release of recombination energy–energy conservation; this scheme is validated for a homogeneous plasma environment (Sec. 3). The simulation results of the expansion of a recombining plasma are then contrasted with the recombination-free case to exemplify its effects (Sec. 4).

2. System and simulation

A total number of N_0 singly-charged ions (mass M, charge $+e$) and N_0 electrons (mass m, charge $-e$) are desorbed from a planar surface between time $t = 0$ and τ. To be specific, all simulation results will be presented for the case of Al ($M =$ 27 amu), i.e. $M/m \cong 4.9 \times 10^4$. No desorption takes place before and after this

https://doi.org/10.1017/S0022377804003332 Published online by Cambridge University Press

period of time, while during this time the desorption flux is constant. We assume that the electron and ion flux densities are the same magnitude, J, in order to leave the ablation target electrically neutral. We furthermore assume that the phase space density $f_0(x = 0, \mathbf{v}, t)$ of the ions immediately after desorption outside the surface is given by the distribution

$$f_0(x = 0, \mathbf{v}, t) = 2n_0 \left(\frac{2M}{\pi k_\mathrm{B} T_0}\right)^{3/2} \exp\left(-\frac{M\mathbf{v}^2}{2k_\mathrm{B}T_0}\right), \quad v_x > 0, \tag{1}$$

for $0 < t < \tau$. Here v_x is the velocity in the x-direction, i.e. perpendicular to the surface. Furthermore, T_0 is the surface temperature, k_B is Boltzmann's constant, and n_0 is the number density of ions immediately outside the surface. Equation (1) assumes a so-called half-Maxwellian distribution perpendicular to the surface, while a Maxwellian distribution of ions and electrons with temperature T_0 is assumed in the directions parallel to the surface. We note that the average ion velocity in the direction perpendicular to the surface is $v_0 = \sqrt{2k_\mathrm{B}T_0/\pi M}$, and the desorbing particle flux density is

$$J = \int f_0(x = 0, \mathbf{v}, t) v_x \, d^3v = n_0 v_0. \tag{2}$$

For the electrons we also assume a half-Maxwellian, i.e. thermal, emission distribution with identical temperature T_0. We note that the electron density in front of the target (immediately after emission) is small, $n_{0,\mathrm{e}} = \sqrt{m/M} n_0 = 4.5 \times 10^{-3} n_0$.

Since the ablation target does not charge up, its electrical potential Φ stays constant; thus we may set $\Phi(x = 0) = 0$ at all times. This means, in particular, that we assume that all particles that return to the surface are reflected from it. Since the total numbers of ions and electrons emitted from the surface are identical, the electrical field $\mathscr{E}$ at the surface and at infinity are connected by Poisson's equation,

$$\mathscr{E}(x = 0) = \mathscr{E}(x = \infty) - \frac{e}{\epsilon_0} \int_0^\infty [n_\mathrm{i}(x) - n_\mathrm{e}(x)] \, dx. \tag{3}$$

We assume that the field at infinity vanishes, $\mathscr{E}(x \to \infty) = 0$; otherwise, ions will be accelerated to arbitrarily high velocities. Hence, $\mathscr{E}(x = 0) = 0$.

We employ the PIC code to solve the coupled plasma expansion problem formulated above. This code is a well-known tool [25–27] for simulating plasma-physics problems and has been applied to a vast variety of problems, cf. [12, 28–30]. Technical details of the application of this code to the plasma emission and expansion problem have been published elsewhere [11, 12]. We mention that the code is spatially one-dimensional, i.e. only the distance x of particles to the emitting wall is included; velocities, however, are included three-dimensionally. For the cases simulated here (cf. Sec. 3.3) we employ a total number of ions (and electrons) $N_0 = 4.3 \times 10^4$, a time step $\Delta t = 2 \times 10^{-5} \tau$, and a spatial cell size of $\Delta x = 0.045 v_0 \tau$; in the cell adjacent to the wall the number of ions reaches 5000 in the course of the simulation. The simulations follow the plasma expansion up to time $t = 6\tau$.

However, we explicitly mention that in addition to the introduction of recombination processes – to be discussed in Sec. 3 – and the action of the self-consistent electrical fields, no collisions have been taken into account. Collisions between different species will, in general, lead to an equilibration between these subsystems, such that their flow velocities and temperatures adapt to each other (modelled as 'friction' in hydrodynamic approaches); furthermore, collisions may lead to a faster

https://doi.org/10.1017/S0022377804003332 Published online by Cambridge University Press

equilibration within each subsystem. In the present paper, we want to emphasize the effects of recombination processes and hence ignore all further collision processes. We note that an exemplary case of the effect of ion–neutral collisions has been studied in [31].

We note that due to recombination, neutral particles enter as another species in our code. Due to the neglect of collisions, their treatment in the simulation is straightforward: they are simply transported with constant velocity. We note, however, that the inclusion of ion–neutral and neutral–neutral collisions will lead to an acceleration of the neutrals away from the surface; the effects of collisions on the expansion of a neutral gas cloud have been well studied in the past [32–34].

Without recombination events, the code is strictly one-dimensional, i.e. only the velocity v_x in the x-direction (normally directed away from the surface) needs to be considered. Velocity components parallel to the surface are unchanged. However, when recombination processes are included, we need to incorporate velocities three-dimensionally, while space may still be treated one-dimensionally.

3. Modelling of three-body recombination

The importance of recombination processes in expanding plasmas has been stressed in several experimental papers, which report on the energy, angle and charge distribution in expanding laser-induced plasmas [35]. Available theoretical analyses, however, concentrate on the temporal evolution of charge states and their energies in a homogeneous plasma (zero-dimensional approach) [36].

3.1. Known characteristics

The process of three-body electron–ion recombination

$$i + e_1^- + e_2^- \rightarrow n + e_2^{-\prime} \tag{4}$$

is governed by the equilibrium rate equation

$$\frac{dn_\mathrm{n}}{dt} = -\frac{dn_\mathrm{i}}{dt} = -\frac{dn_\mathrm{e}}{dt} = k n_\mathrm{e}^2 n_\mathrm{i}, \tag{5}$$

where n_ν is the particle number density of species ν (ν = n, i, e, for neutrals, ions, electrons) and k is the rate constant. It is assumed that electron 1 neutralizes the ion, while electron 2 escapes, carrying off the excess energy. Since the recombination process is governed by Coulomb collisions, the rate constant exhibits a strong dependence on the particle energies, which is usually [37] parametrized by the electron temperature T_e as

$$k = B T_\mathrm{e}^{-4.5}. \tag{6}$$

We call B the rate coefficient; it depends on the ion species via its ionization and excitation energies. The $T_\mathrm{e}^{-4.5}$-dependence is a general feature of three-body recombination, valid for not too high electron temperatures, $k_\mathrm{B} T_\mathrm{e} \ll E_\mathrm{i}$, where E_i is the ionization energy.

Energy conservation in the recombination process demands

$$E_\mathrm{i} + E_{\mathrm{e},1} + E_{\mathrm{e},2} + E_\mathrm{rec} = E_\mathrm{n} + E'_{\mathrm{e},2}, \tag{7}$$

where E_ν is the kinetic energy of particle ν. E_rec is the recombination energy, i.e. the potential energy stored in the ion–electron system that is released upon recombination. It is $E_\mathrm{rec} > 0$. In the simplest approximation E_rec may be set equal

https://doi.org/10.1017/S0022377804003332 Published online by Cambridge University Press

to the ionization energy; however, its value will decrease if excited levels become populated.

In a thermal plasma, where electrons and ions have roughly the same energy, due to the tiny electron mass, electrons carry negligible momentum compared with ions. Hence, momentum conservation in (7) demands that the neutral atom carries essentially the same velocity as the ion. Hence,

$$E_{\mathrm{n}} \cong E_{\mathrm{i}}. \tag{8}$$

We conclude that

$$E'_{\mathrm{e},2} \cong E_{\mathrm{e},1} + E_{\mathrm{e},2} + E_{\mathrm{rec}}. \tag{9}$$

Thus, recombination processes heat the electron subsystem by two processes:

(1) by *energy concentration*, i.e. the energies of two electrons are imparted to the escaping electron, which on average it attains $2k_{\mathrm{B}}T_{\mathrm{e}}$; and

(2) by the release of recombination energy.

3.2. Simulation model

The collision kinematics of a three-body recombination event are as follows. If an ion with velocity $\mathbf{V}$ and two electrons with velocities $\mathbf{v}_1$ and $\mathbf{v}_2$ collide, the resulting neutral has velocity

$$\mathbf{V}' = \frac{(m+M)\mathbf{V}^* + m\mathbf{v}_2}{M+2m} - \gamma\frac{m}{M+2m}v_{\mathrm{rel},2}\mathbf{n}, \tag{10}$$

and the released electron has velocity

$$\mathbf{v}'_2 = \frac{(m+M)\mathbf{V}^* + m\mathbf{v}_2}{M+2m} + \gamma\frac{M+m}{M+2m}v_{\mathrm{rel},2}\mathbf{n}. \tag{11}$$

Here, $\mathbf{V}^* = (m\mathbf{v}_1 + M\mathbf{V})/(m+M)$ is the velocity of the intermediary excited neutral, $v_{\mathrm{rel},2}$ is the relative velocity between electron 2 and the intermediary excited neutral, and γ is a kinematical factor,

$$\gamma = \sqrt{1 + \frac{E_{\mathrm{rel},1}}{E_{\mathrm{rel},2}} + \frac{E_{\mathrm{rec}}}{E_{\mathrm{rel},2}}}. \tag{12}$$

$E_{\mathrm{rel},1}$ ($E_{\mathrm{rel},2}$) denotes the relative energy between electron 1 (2) and the intermediary excited neutral, and $\mathbf{n}$ is a unit vector that is chosen randomly on the surface of the unit sphere with uniform distribution.

Since recombination is a three-body collision event, it is not easily included in a kinetic code, which is based on a strict separation of transport in the self-consistent field and collisions. We include it by performing in each cell the following routine during each PIC time step Δt. We set the collision time counter t_{c} to zero. In a cell containing N_{i} ions and an electron density n_{e}, the number of recombination events occurring in Δt is $N_{\mathrm{i}}n_{\mathrm{e}}^2 k\Delta t$. Hence, the collision frequency is

$$\nu_{\mathrm{c}} = N_{\mathrm{i}}n_{\mathrm{e}}^2 k. \tag{13}$$

Following the null-collision technique [27, 38, 39], we fix the maximum electron velocity to $v_{\max} = 30v_{\mathrm{th}}$, where $v_{\mathrm{th}} = \sqrt{8k_{\mathrm{B}}T_{\mathrm{e}}/\pi m}$ is the thermal electron velocity. Assuming, as in two-body collisions, that the collision frequency is proportional to the relative velocity, this corresponds to a maximum collision frequency $\bar{\nu}_{\mathrm{c}} = N_{\mathrm{i}}n_{\mathrm{e}}^2 k v_{\max}/v_{\mathrm{th}}$.

https://doi.org/10.1017/S0022377804003332 Published online by Cambridge University Press

We advance the time counter by dt_c, a random number that is exponentially distributed around its mean $1/\bar{\nu}_e$. If $t_c + dt_c > \Delta t$, then no further collisions occur in this cell, and the routine leaves the cell. Otherwise, we choose an ion and two electrons at random and let them collide depending on the probability $v_{rel,2}/v_{max}$. As usual, the advantage of the null-collision method is that the collision frequency does not need to be evaluated individually at each time step in each cell.

In order to check the validity of the code, we simulated the recombination behavior in a homogeneous plasma with a three-dimensional Maxwellian electron and ion distribution with initial temperature T_0 [40]. The time evolution of electrons, ions and the number of recombinations then follows the solution of (5) with a rate k that is identical to the prescribed rate. This proves that our algorithm recovers the correct macroscopic three-body recombination frequency.

Previous attempts of including three-body recombination into the PIC-code either use an unrealistic electron-temperature dependence [24] or rely on distorting the electron distribution function to make it strongly divergent towards zero energy [23].

The present approach is not suited to predicting the shape of the electron distribution function. However, we are confident that our results allow a detailed assessment of the qualitative changes in the expanding plasma cloud, the recombined neutral gas cloud, and the electrical fields that accelerate the ions.

3.3. Scaling

If no recombinations occur, it is known [11] that the plasma expansion problem is governed by two parameters, m/M and $\xi = \sqrt{2/\pi}\tau\omega_i$, where $\omega_i = \sqrt{n_0 e^2/M\epsilon_0}$ is the ion plasma frequency. The latter parameter can also be written as $\xi = v_0\tau/\lambda$, with $\lambda = \sqrt{\epsilon_0 kT_0/n_0 e^2}$ the Debye length of the plasma. Since $m \ll M$, and m/M can be assumed fixed, only the second parameter can be chosen freely in an experiment by adjusting the laser pulse duration τ; it has been chosen as $\xi = 6$ in the present study.

The recombination process introduces two further scaling parameters. The first is $\alpha_{rec} = 1 - (1 + 2n_0^2 k\tau)^{-1/2}$ and is a measure of the probability that an ion recombines during the emission phase. This expression originates from solving (5) in a homogeneous plasma ($n_e = n_i = n_0$) with constant temperature. The exact recombination probability is of course a more complex quantity, since the electron density and temperature vary with time and space and need to be calculated self-consistently in the simulation (cf. our results in Fig. 2). In our study we chose $\alpha_{rec} = 0.75$. This, rather high, recombination probability has been chosen in this model study in order to clearly identify the effects of recombination in an expanding plasma.

Plasmas with different values of kT_e, n_0, τ correspond to the scaling parameters adopted in this study. As an example, we mention a plasma characterized by $kT_e = 1$ eV, $n_0 = 9 \times 10^{24}$ m^{-3} and a laser pulse duration $\tau = 10$ ps. Here, for the calculation of the recombination rate, we use a rate coefficient $B = 9 \times 10^{-39}$ m^6 s^{-1}, if T_e is measured in electronvolts [2, 41].

The second new parameter is $E_{rec}/k_B T_0$ and measures the relative influence of the recombination energy. We present two simulations, one with $E_{rec} = 0$ and another with $E_{rec} = 36 k_B T_0$ as an extreme case.

https://doi.org/10.1017/S0022377804003332 Published online by Cambridge University Press

4. Results: recombination in an expanding plasma

In this section we study the effects of recombinations on the expansion of a plasma containing a single ion-charge state. To this end, we perform three simulations:

(1) a recombination-free expansion, which will serve as a reference case;

(2) an expansion for an energy-conserving recombining plasma, in which the recombination energy $E_{\rm rec} = 0$;

(3) an exothermally recombining expansion, $E_{\rm rec} > 0$ – we chose a large value $E_{\rm rec}/k_{\rm B}T_0 = 36$ as an extreme case.

4.1. Global properties of the expansion: energies

To get an overview over the effects of recombination, we first study the energy in the plasma cloud. We normalize energies to the total energy of ions emitted from the wall

$$E_0 = \frac{N_0}{J} \int \frac{M}{2} \mathbf{v}^2 f_0(x=0,\mathbf{v},t) v_x \, d^3v = 2k_{\rm B}T_0 N_0, \tag{14}$$

where N_0 is the number of ions emitted. Equation (14) is a result of the fact that in our model each electron and ion is emitted with a half-Maxwellian distribution characterized by the wall temperature T_0. As a consequence, each electron and ion carries the energy $\int (M/2) {v_x}^2 f_0(x=0,\mathbf{v},t) v_x \, d^3v/J = k_{\rm B}T_0$ in the direction of flow, and the same energy in the direction perpendicular to the flow, $\int (M/2)({v_y}^2 + {v_z}^2) f_0(x=0,\mathbf{v},t) v_x \, d^3v/J = k_{\rm B}T_0$.

Figure 1 shows the time evolution of the kinetic energies of ions, $E_{\rm i}$, of electrons, $E_{\rm e}$, and of neutrals, $E_{\rm n}$, during the flow. Furthermore, the potential energy in the system

$$E_{\rm pot} = \frac{1}{2} \int dx \, \rho(x) \Phi(x) \tag{15}$$

is displayed, where $\rho = e[n_{\rm i}(x) - n_{\rm e}(x)]$ is the space-charge density and Φ is the potential.

Figure 1(a) shows our results for the recombination-free expansion. For $0 < t < \tau$, $E_{\rm tot}$ rises linearly due to the ongoing emission. Note that, if no fields were present, $E_{\rm e} = E_{\rm i} = E_0 = 2k_{\rm B}T_0N_0$ at all times $t > \tau$. The effect of the space-charge fields building up during the expansion is to transfer energy from the electronic to the ionic subsystem. Due to the planar geometry of the expansion, the energy perpendicular to the flow is conserved,

$$E_{\rm i}^{\perp} = E_{\rm e}^{\perp} = \tfrac{1}{2} E_0 = \text{constant}, \tag{16}$$

since the one-dimensional PIC code treats electrons and ions as charge sheets rather than point particles. Here the inclusion of Coulomb angular scattering would act to isotropize the angular distributions of electron energy and hence to change (16). Figure 1(a) thus essentially shows that the electrons give away all their energy in flow directions to the ions; this result is well known, cf. [11].

Figure 1(b) displays the analogous data for the energy-conserving recombining flow. The total energy shows exactly the same behaviour as in Fig. 1(a), thus proving the conservation of energy in the simulation. However, the distribution of the total energy on the various particle species is strongly changed. The main difference is that a considerable fraction of the energy is now given to the neutrals that are

https://doi.org/10.1017/S0022377804003332 Published online by Cambridge University Press

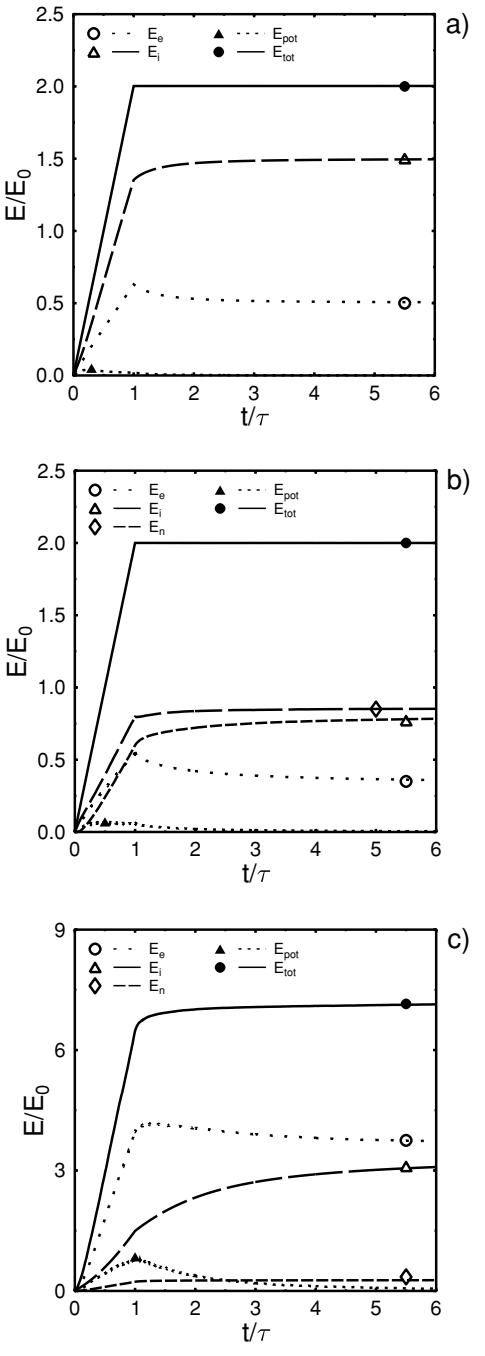


Figure 1. Time evolution of the total energy $E_{\rm tot}$ in the expansion, and of its contributions: kinetic energy of ions, $E_{\rm i}$, electrons, $E_{\rm e}$, and neutrals, $E_{\rm n}$ as well as potential energy, $E_{\rm pot}$. Energies are normalized to the total energy of ions upon emission, $E_0 = 2k_{\rm B}T_0N_0$. (a) Recombination-free expansion; (b) recombining expansion, $E_{\rm rec} = 0$; (c) exothermal recombining expansion, $E_{\rm rec} > 0$.

https://doi.org/10.1017/S0022377804003332 Published online by Cambridge University Press

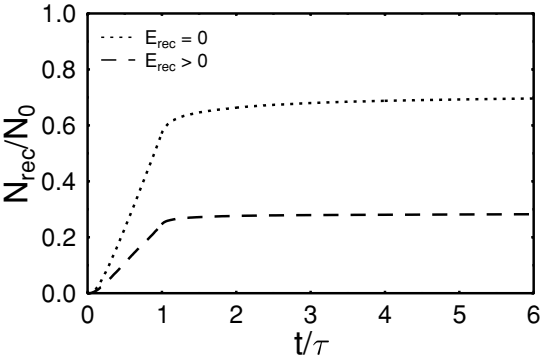


Figure 2. Time evolution of total number of recombinations, $N_{\rm rec}$, occurring during expansion, normalized to the total number of emitted ions, N_0.

formed in the recombination processes. As a consequence, ion and electron energies are smaller than in the reference case, Fig. 1(a).

If a non-zero recombination energy $E_{\rm rec}$ is included, the situation changes again, cf. Fig. 1(c). First of all, the total energy is substantially higher than in the previous cases; this is of course due to the energy liberated upon recombination. Then, electrons now carry the major part of the energy, while the energy possessed by the neutrals becomes negligible. Note also that the potential energy in the system has substantially increased.

For a further discussion of the energies in the system, it is necessary to study the change in the particle numbers first. They are conveniently expressed by the number of neutrals formed, $N_{\rm n}(t)$, which is identical to the number of recombination events happening until time t, $N_{\rm rec}(t)$,

$$N_{\rm rec}(t) = N_{\rm n}(t) = N_0 - N_{\rm e}(t) = N_0 - N_{\rm i}(t). \tag{17}$$

Figure 2 shows the time dependence of this quantity, normalized to the total number of ions emitted, N_0; thus, $N_{\rm rec}/N_0$ equals the probability that an ion neutralizes during the expansion. We observe that the exothermal energy release in the flow decreases $N_{\rm rec}$; this is due to the inverse temperature dependence of the recombination rate (6). Figure 2 also demonstrates that the major part of the recombination events happen during the emission phase, $t < \tau$; in the two simulations presented, only few recombinations occur in the post-emission phase, $t > \tau$. Note that the total recombination probability amounts to 70%, and is thus in good agreement with the scaling parameter $\alpha_{\rm rec}$, cf. Sec. 3.3.

A key quantity of our study is the (normalized) energies per particle

$$\epsilon_\nu = \frac{E_\nu}{2k_{\rm B}T_0 N_\nu(t)} = \frac{E_\nu/E_0}{N_\nu/N_0}, \quad \nu = {\rm e, i, n}, \tag{18}$$

which may be evaluated for the ion (i), electron (e), and neutral (n) subsystems; for the potential energy, we normalize to the instantaneous number of ions, $N_{\rm i}(t) = N_{\rm e}(t)$.

Figure 3(a) demonstrates again the space-charge-induced acceleration process by which the electron energy in the direction of flow is converted into ion energy. Figure 3(b) in addition shows the effect of *energy concentration*: due to the diminishing number of particles during the flow process – at the end of the simulation

https://doi.org/10.1017/S0022377804003332 Published online by Cambridge University Press

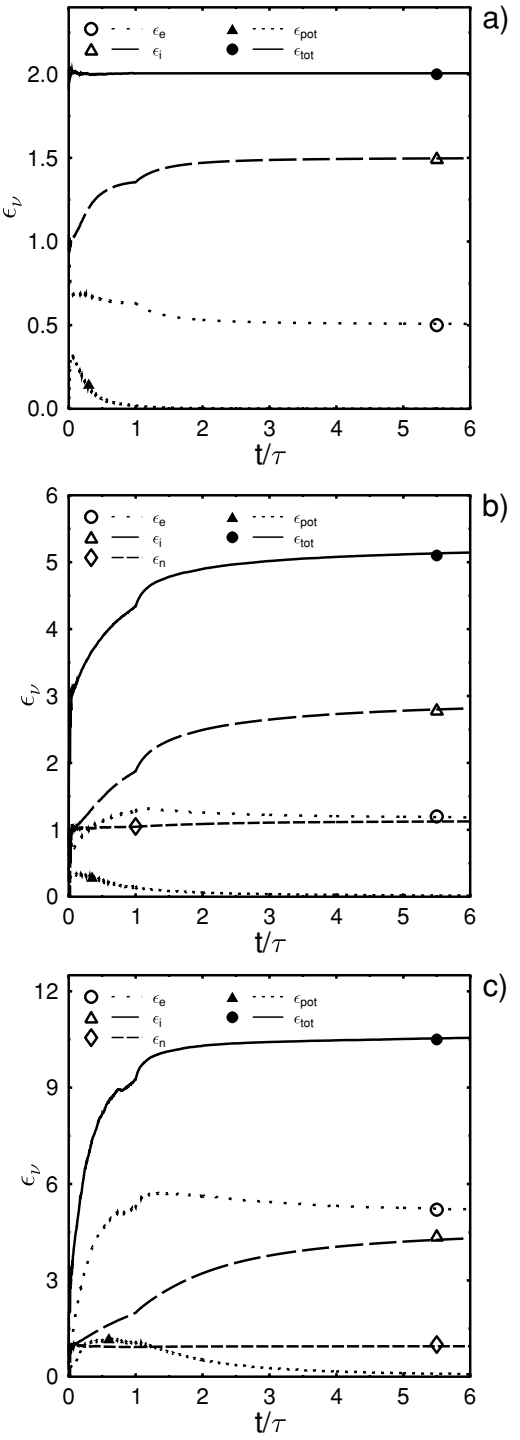


Figure 3. Time evolution of the normalized energies per particle ϵ_ν (18). (a) Recombination-free expansion; (b) recombining expansion, $E_{\rm rec} = 0$; (c) exothermal recombining expansion, $E_{\rm rec} > 0$.

https://doi.org/10.1017/S0022377804003332 Published online by Cambridge University Press

$t = 6\tau$, only 30% of the emitted ions and electrons have survived – the constant total energy is distributed among fewer particles; hence, the energy per particle strongly increases. Note that due to the kinematics of the three-body collision process, cf. (10) and (11), the energy of ions and neutrals perpendicular to the flow remains essentially unchanged,

$$E_{\mathrm{i}}^{\perp} = E_{\mathrm{n}}^{\perp} \cong \tfrac{1}{2} E_0 = \text{constant} \tag{19}$$

Hence, Fig. 3 demonstrates that the energy in the direction of flow of an ion has increased from roughly $E_0 = 2k_{\mathrm{B}}T_0$ in the recombination-free flow (Fig. 3(a)) to $2.25E_0 = 4.5k_{\mathrm{B}}T_0$ due to recombinations (Fig. 3(b)). The energy of neutrals is more or less constant $E_{\mathrm{n}} = 2k_{\mathrm{B}}T_0$, i.e. it corresponds to the emission distribution of ions. We note that the electron energy $E_{\mathrm{e}} = 2.4k_{\mathrm{B}}T_0$ at the end of the flow consists almost exclusively of electron energy transverse to the flow, $2.2k_{\mathrm{B}}T_0$, while the electron energy parallel to the flow is only $0.2k_{\mathrm{B}}T_0$; this value is higher than in the recombination-free case, but still negligible.

The situation changes again when the energy release during recombination is taken into account, Fig. 3(c). Even though in this case fewer recombination events occur, the heating of the electron component is substantial. A closer analysis shows that again the major part of the electron energy (95%) is in the direction transverse to the flow. The ion energy in the direction of flow is $7.6k_{\mathrm{B}}T_0$.

Note that for recombining flows (Figs. 3(b) and 3(c)) the potential energy at the end of the simulation is not yet zero, indicating that further acceleration processes happen after $t = 6\tau$. This is due to the recombination heating of the electronic subsystem.

4.2. Local properties: ion acceleration

Figure 4 shows the space dependence of the ion velocities at the end of the emission phase, $t = \tau$, and in the post-emission phase, $t = 6\tau$, for the three cases studied. We observe a rather linear increase $u \propto x/t$; only slight deviations from this linear law occur if recombinations are included in the simulation. The highest ion velocities are attained at the expansion front. Their values increase when recombination is taken into account, and with the size of the recombination energy. This finding is in agreement with the average ion energy discussed in Fig. 3.

Figure 5 shows the ion and electron spatial distribution at the end of the emission phase, $t = \tau$, from which we can read off the resulting space charge. At this moment, $t = \tau$, space charges are strongest; after emission, the plasma bulk quickly becomes quasi-neutral and space charges will only remain at the expansion front. A general feature seen in all simulations is that, while the ions form a rather well defined ion front at around $x \cong (5-6)v_0\tau$, electrons expand further out into the vacuum; this creates the expansion-front space-charge electrical field, which is the prime cause of ion acceleration. Note that in all cases the ion front is characterized by a double-layer structure, which is most pronounced in the exothermally recombining flow (Fig. 5(c)).

Recombination has a strong effect on the charge distribution close to the surface. In this region, recombinations occur most frequently; hence the ion density drops sharply. Electrons, however, retain an exponential spatial profile attempting to keep the bulk of the plasma cloud quasi-neutral. As a consequence the region immediately adjacent to the surface becomes positively charged in the recombining

https://doi.org/10.1017/S0022377804003332 Published online by Cambridge University Press

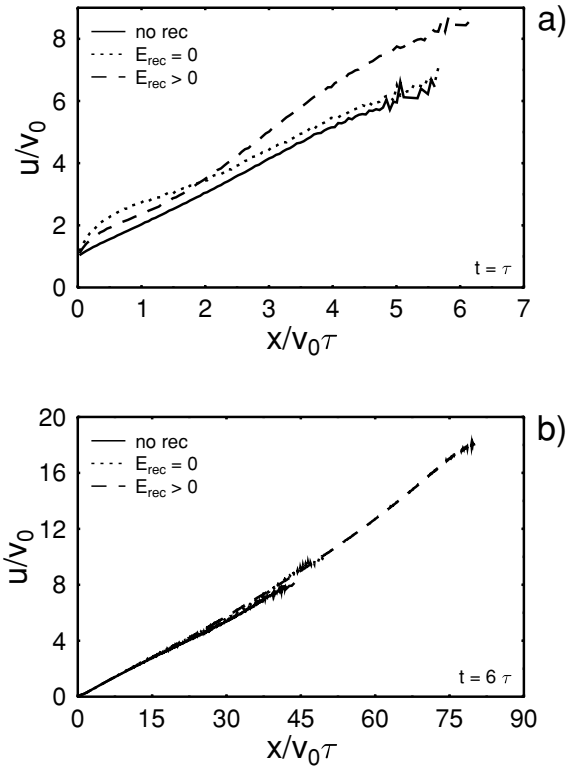


Figure 4. Space dependence of ion velocity u (a) at the end of the emission phase, $t = \tau$, and (b) in the post-emission phase, $t = 6\tau$.

flows. This is compensated for by a slightly negative space-charge region following at $x \cong v_0\tau$.

Figure 6 shows the electrical field in the plasma cloud originating from the space charges analysed above. The natural scale of the field in a self-similar expansion is [12]

$$\mathscr{E}_0 = \frac{2}{\pi}\sqrt{\frac{k_B T_0 n_0}{\epsilon_0}}. \tag{20}$$

The main feature is the strong ion-accelerating field at the expansion front resulting from the double-layer structure described above. Its strength increases with increasing electron temperature, i.e. from the recombination-free flow over the energy-conserving recombining flow to the exothermal recombining flow (cf. Fig. 9 below). The second space-charge field immediately in front of the surface, which is due to the near-surface double layer described above and has its origin in the recombination processes occurring there, is clearly visible and helps in accelerating ions off the surface.

A simple self-similar model available for the expansion of a fully ionized plasma into a vacuum predicts [12] the field to be homogeneous and to decay in time as $\mathscr{E}(x,t) = \mathscr{E}_0\tau/\xi t$. This prediction has been shown to give a reasonable order-of-magnitude estimate of the strength of the field in the expanding plasma cloud. In

https://doi.org/10.1017/S0022377804003332 Published online by Cambridge University Press

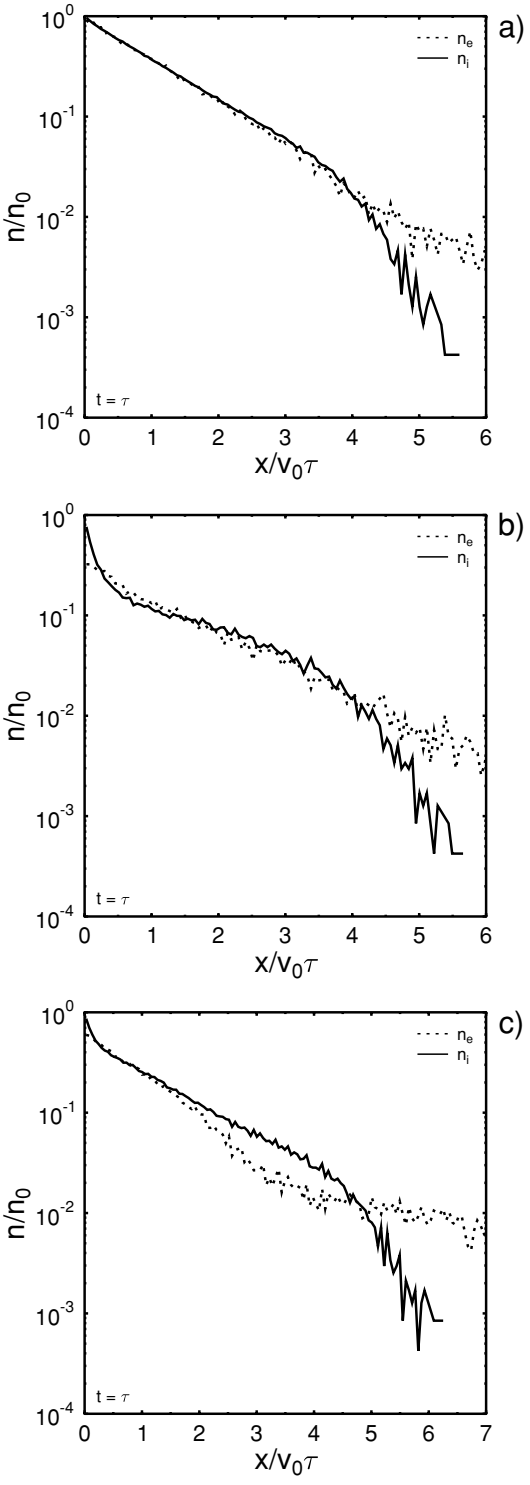


Figure 5. Space dependence of the ion density n_i and electron density n_e at the end of the emission phase, $t = \tau$. (a) Recombination-free expansion; (b) recombining expansion, $E_\mathrm{rec} = 0$; (c) exothermal recombining expansion, $E_\mathrm{rec} > 0$.

https://doi.org/10.1017/S0022377804003332 Published online by Cambridge University Press

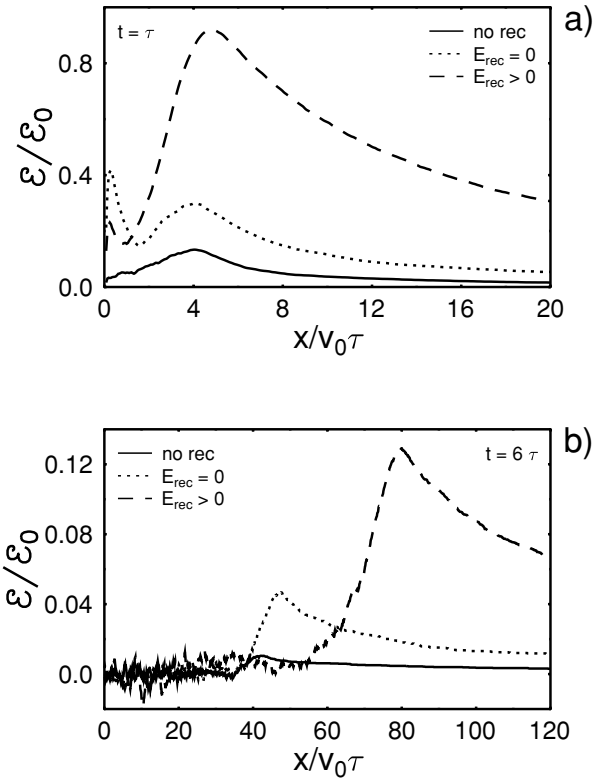


Figure 6. Space dependence of electrical field $\mathscr{E}$, normalized to the self-similar scale $\mathscr{E}_0$, (a) at the end of the emission phase, $t = \tau$, and (b) in the post-emission phase, $t = 6\tau$.

order to take the strongly increasing electron temperature in a recombining plasma into account, we scale the field with

$$\mathscr{E}'_0 = \mathscr{E}_0 \sqrt{\frac{T_\mathrm{e}}{T_0}}, \tag{21}$$

where the electron temperature T_e is evaluated at the position where the field is maximum, i.e. in the expansion front. We thus extend the self-similar model prediction to give

$$\mathscr{E}(x,t) = \mathscr{E}'_0 \frac{\tau}{\xi t} = \mathscr{E}'_0 \frac{\lambda}{v_0 t}. \tag{22}$$

Figure 7 shows that this scaling gives a reasonable estimate of the strength of the space-charge field in the three cases studied.

Figure 8 displays the temporal decay of the maximum of the electrical field in the expansion front in the post-emission phase. The decay can be fitted by a $1/t$-dependence also after emission. The case of a non-recombining plasma, for early times $\tau < t \lesssim 4\tau$, is the only case where the decay is stronger, $\propto t^{-1.6}$. The slow decay visible in our simulation proves that the space-charge acceleration persists long after the emission phase and will be able to accelerate particles to high

https://doi.org/10.1017/S0022377804003332 Published online by Cambridge University Press

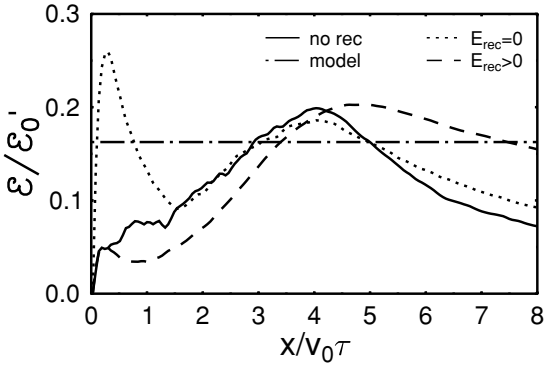


Figure 7. Space dependence of the electrical field $\mathscr{E}$ in the emission phase, $t = \tau$. Data of Fig. 6(a) rescaled to $\mathscr{E}'_0$ given by (21). Model prediction: (22).

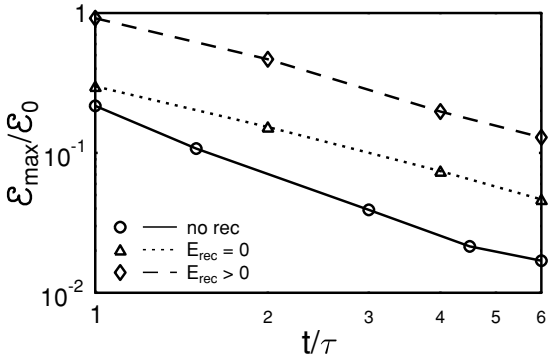


Figure 8. Temporal decay of the maximum of the electrical field, $\mathscr{E}_{\max}$, in the expansion front in the post-emission phase.

velocities. We note that in an earlier study [4], it was argued that ions can indeed attain velocities up to the electron thermal velocity.

Figure 9 shows the spatial distribution of the electron temperature at the end of the expansion phase. As usual, temperature is defined via the kinetic energy of random motion around the average local electron speed. The electron temperature is rather constant throughout the plasma cloud, and decays only at a larger distance outwards into the vacuum. This is due to the high mobility of the electrons. The pronounced rise of the electron temperature as soon as recombinations are introduced (Fig. 9(b)) and, in particular, when the energy released upon recombination is taken into account (Fig. 9(c)) is clearly visible.

In order to study the places where recombinations occur, Fig. 10 shows the space distribution of the recombination rate, $N_{\rm rec}(x)$. Since most recombinations occur in the emission phase (cf. Fig. 2), these recombinations occur adjacent to the surface, $0 < x \lesssim v_0\tau$. The remaining recombinations occur in the expanding plasma cloud. Note that these latter processes are strongly suppressed for the exothermally recombining flow, due to the high electron temperature there (cf. (6)).

https://doi.org/10.1017/S0022377804003332 Published online by Cambridge University Press

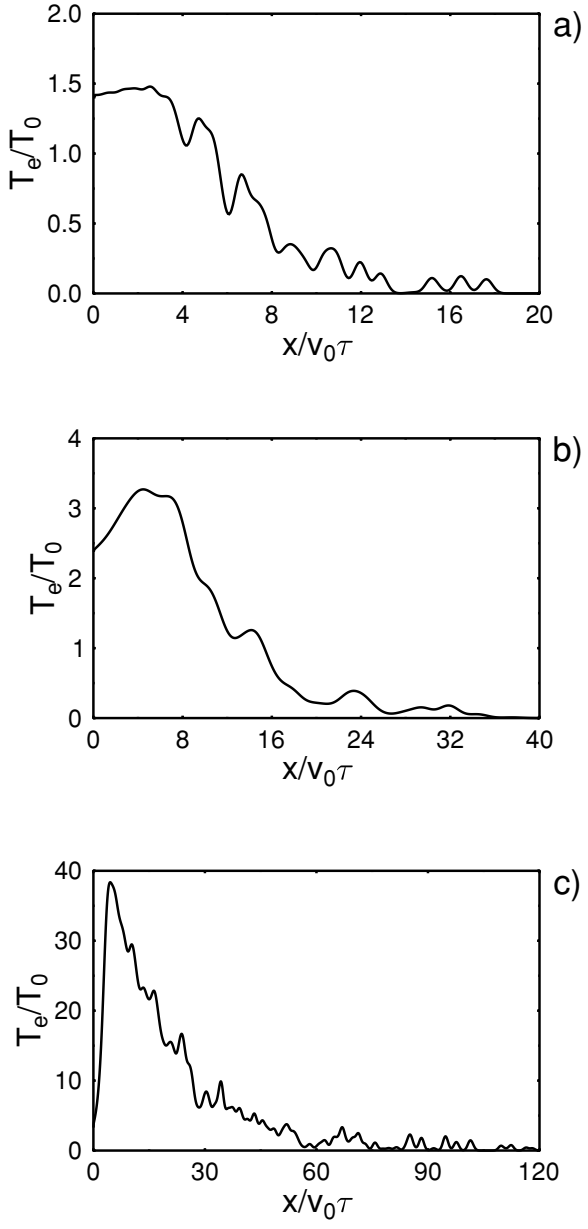


Figure 9. Space dependence of the electron temperature T_e at the end of the emission phase, $t = \tau$. (a) Recombination-free expansion; (b) recombining expansion, $E_{rec} = 0$; (c) exothermal recombining expansion, $E_{rec} > 0$. Note the change in abscissa scale.

In Fig. 11 we show the spatial segregation of the plasma cloud (n_i) and the gas cloud (n_n) in the post-emission phase, $t = 6\tau$. Note, in particular, the high acceleration of the ions that results in the large distance of the ion front from the wall in the case of the exothermally recombining flow. The exponential ion profile for the non-recombining flow becomes less steep due to recombinations (Fig. 11(b)), and almost flat in Fig. 11(c).

https://doi.org/10.1017/S0022377804003332 Published online by Cambridge University Press

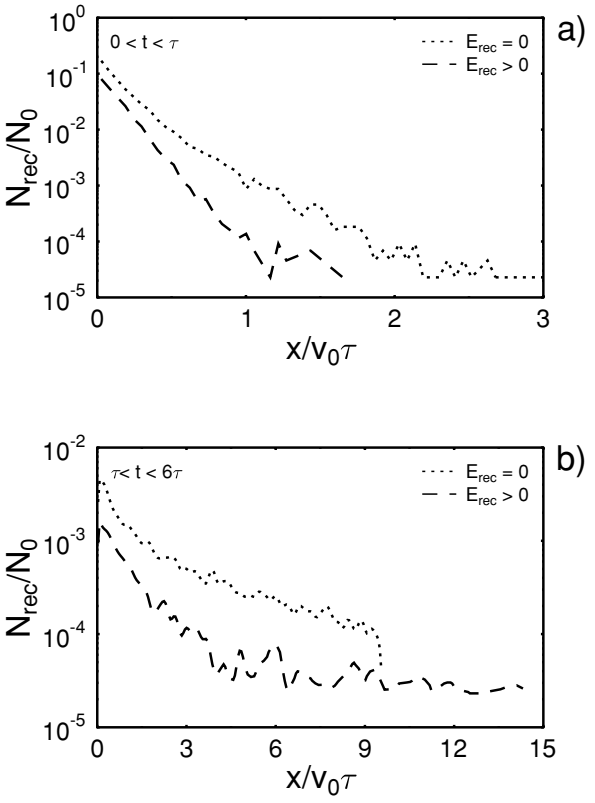


Figure 10. Space dependence of the total number of recombinations, $N_{\rm rec}$, occurring (a) in the emission phase, $0 < t < \tau$, and (b) in the post-emission phase, $\tau < t < 6\tau$.

5. Summary

(1) We have studied the expansion of a plasma formed by thermal evaporation of ions and electrons off a planar wall into a vacuum with the kinetic PIC code. Three-body recombination processes are implemented via a simple scheme, which takes into account energy and momentum conservation during the process, and reproduces the well-known density and temperature dependence of the recombination rate.

(2) In this scheme, the expansion essentially depends on two dimension-free parameters: the average fraction of neutralized ions, $\alpha_{\rm rec}$, and the recombination energy released, relative to the ion evaporation temperature, $E_{\rm rec}/k_{\rm B}T_0$.

(3) Recombination concentrates the energy in the expansion flow on fewer particles. As a consequence, the energy per particle increases. This *energy concentration* process is further amplified by the release of the recombination energy of the flow.

(4) During the flow, the expansion energy is transferred to a large extent to ion acceleration. As a consequence, the kinetic energy of ions increases considerably above its value upon emission. The mechanism is as follows: due to recombination, the electron temperature $T_{\rm e}$ strongly increases. As a consequence, the

https://doi.org/10.1017/S0022377804003332 Published online by Cambridge University Press

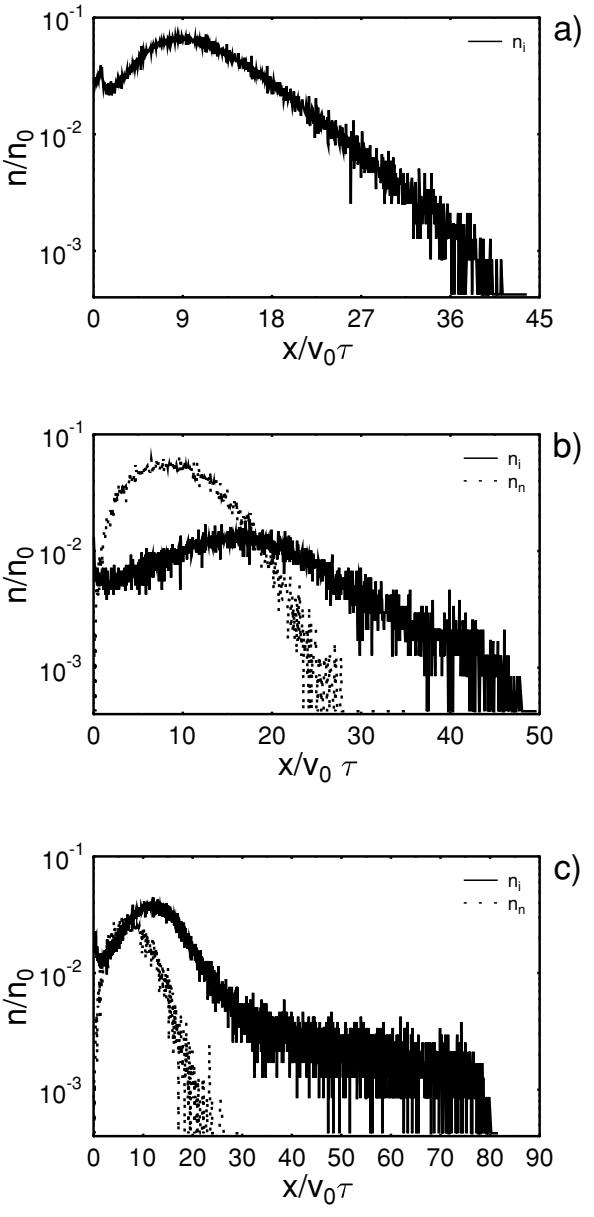


Figure 11. Ion density n_i (full) and neutral density n_n (dashed) in the post-emission phase, $t = 6\tau$. (a) Recombination-free expansion; (b) recombining expansion, $E_\mathrm{rec} = 0$; (c) exothermal recombining expansion, $E_\mathrm{rec} > 0$.

space-charge field which builds up at the expansion front increases as $\sqrt{T_\mathrm{e}}$, and ions are accelerated.

(5) The shape of the plasma cloud is distorted by the ion acceleration, and develops a long tail towards the vacuum side. Furthermore, spatial segregation of the plasma cloud and the neutral gas cloud sets in.

https://doi.org/10.1017/S0022377804003332 Published online by Cambridge University Press

(6) The electrical field in the expansion front decays only slowly, as $1/t$ with time in the post-emission phase. Due to this slow decay, ions can attain considerable velocities even after emission has terminated.

(7) The results obtained in this work give qualitative support to the 'recombination model' [10, 18, 36, 42] of charge-state segregation and differential ion acceleration in expanding plasmas. This model assumes a dominant role of three-body recombination processes on the segregation of a plasma cloud into its various charge-state components, which has often been observed experimentally [1–3, 13–15, 35, 42, 43]. An extension of our PIC simulation work to include several ion charge states is available [44].

Acknowledgements

We thank K. Rohr for discussions. Support by the Deutsche Forschungsgemeinschaft is gratefully acknowledged.

References

[1] Hughes, T. P. 1975 *Plasmas and Laser Light*. Bristol: Hilger.
[2] Phipps, C. R. and Dreyfus, R. W. 1993 *Laser Ionization Mass Analysis (Chemical Analysis, 124)* (ed. A. Vertes, R. Gijbels and F. Adams). New York: Wiley, p. 369.
[3] Bäuerle, D. 2000 *Laser Processing and Chemistry*, 3rd edn. Berlin: Springer.
[4] Gurevich, A. V., Pariiskaya L. V. and Pitaevskii, L. P. 1966 *Sov. Phys.–JETP* **22**, 449.
[5] Crow, J. E., Auer, P. L. and Allen, J. E. 1975 *J. Plasma Phys.* **14**, 65.
[6] Denavit, J. 1979 *Phys. Fluids* **22**, 1384.
[7] Sack, C. and Schamel, H. 1987 *Phys. Rep.* **156**, 311.
[8] Mattioli, M. 1971 *Plasma Phys.* **13**, 19.
[9] Mulser, P. 1971 *Plasma Phys.* **13**, 1007.
[10] Granse, G., Vollmar, S., Lenk, A., Rupp, A. and Rohr, K. 1996 *Appl. Surf. Sci.* **96–98**, 97.
[11] Ellegaard, O., Nedelea, T., Schou, J. and Urbassek, H. M. 2002 *Appl. Surf. Sci.* **197–198**, 229.
[12] Nedelea, T. and Urbassek, H. M. 2002 *Phys. Plasmas* **9**, 3209.
[13] Pitsch, P., Rohr, K. and Weber, H. 1981 *J. Phys.* D **14**, L51.
[14] Rupp, A. and Rohr, K. 1995 *J. Phys.* D **28**, 468.
[15] Chrisey, D. B. and Hubler, G. K. (eds.) 1994 *Pulsed Laser Deposition of Thin Films*. New York: Wiley.
[16] Demtröder, W. and Jantz, W. 1969 *Plasma Phys.* **12**, 691.
[17] Torrisi, L., Gammino, S., Ando, L. and Laska, L. 2002 *J. Appl. Phys.* **91**, 4685.
[18] Goforth, R. R. and Hammerling, P. 1976 *J. Appl. Phys.* **47**, 3918.
[19] Bhattacharya, D. K. and Lie, G. C. 1991 *Phys. Rev. A* **43**, 761.
[20] Larson, D. J. 2003 *J. Comput. Phys.* **188**, 123.
[21] van de Sanden, M. C. M., de Regt, J. M. and Schram, D. C. 1993 *Phys. Rev.* E **47**, 1792.
[22] Ethier, S. and Matte, J. P. 2001 *Phys. Plasmas* **8**, 1650.
[23] Nanbu, K. and Shiozawa, M. 2000 Reports of the Institute of Fluid Science, no. 12, Tohoku University, p. 153.
[24] Nanbu, K. Yonemura, S. and Sasaki, A. 1999 *Japan J. Appl. Phys.* **38**, 4460.
[25] Birdsall, C. K. and Langdon, A. B. 1991 *Plasma Physics via Computer Simulation*. New York: McGraw-Hill.

https://doi.org/10.1017/S0022377804003332 Published online by Cambridge University Press

[26] Hockney, R. W. and Eastwood, J. W. 1994 *Computer Simulation using Particles*. Bristol: Institute of Physics.
[27] Birdsall, C. K. 1991 *IEEE Trans. Plasma Sci.* **19**, 65.
[28] Procassini, R. J. and Birdsall, C. K. 1991 *Phys. Fluids* B **3**, 1876.
[29] Cartwright, K. L., Verboncoeur, J. P. and Birdsall, C. K. 2000 *Phys. Plasmas* **7**, 3252.
[30] Soria, C. 2001 Pontiga, F. and Castellanos, A. *J. Comput. Phys.* **171**, 47.
[31] Nedelea, T. and Urbassek, H. M. 2004 *Phys. Rev.* E **69**, 056408.
[32] Sibold, D. and Urbassek, H. M. 1991 *Phys. Rev.* A **43**, 6722.
[33] Urbassek, H. M. and Sibold, D. 1993 *Phys. Rev. Lett.* **70**, 1886.
[34] Sibold, D. and Urbassek, H. M. 1993 *J. Appl. Phys.* **73**, 8544.
[35] Sinha, B. K., Thum-Jaeger, A. and Rohr, K. P. 1999 *J. Plasma Fusion Res.* **2**, 406.
[36] Kunz, I. 1990 PhD thesis, University Darmstadt.
[37] Lieberman, M. A. and Lichtenberg, A. J. 1994 *Principles of Plasma Discharges and Materials Processing*. New York: Wiley.
[38] Koura, K. 1986 *Phys. Fluids* **29**, 3509.
[39] Boeuf, J. P. and Marode, E. 1982 *J. Phys.* D **15**, 2169.
[40] Nedelea, T. 2004 PhD thesis, University Kaiserslautern.
[41] Zel'dovich, Y. B. and Raizer, Y. P. 1966 *Physics of Shock Waves and High-Temperature Hydrodynamic Phenomena*, vol. 1. New York: Academic Press.
[42] Golubev, A. A., Latyshev, S. V. and Sharkov, B. Y. 1984 *Sov. J. Quantum Electron.* **14**, 1242.
[43] Tallents, G. J. 1980 *Plasma Phys.* **22**, 709.
[44] Nedelea, T. and Urbassek, H. M. 2004 *J. Phys.* D **37**, 2981.

https://doi.org/10.1017/S0022377804003332 Published online by Cambridge University Press